Discrimination of Large Venous Vessels in Time-Course Spiral Blood-Oxygen-Level-Dependent Magnetic-Resonance Functional Neuroimaging

Adrian T. Lee, Gary H. Glover, Craig H. Meyer

A technique is described for discriminating blood-oxygen-level-dependent (BOLD) signal changes originating from large venous vessels and those that arise from the cortical parenchyma based on examining the temporal delay of each pixel's response. Photic stimulation experiments were performed with a conventional 1.5 T scanner and correlated each pixel's time-course with sine and cosine functions at the frequency of the stimulus. It was found that the signal in pixels anatomically associated with gray matter was delayed between 4 and 8 s compared with the stimulus, whereas the signal in pixels correlated with visible vessels and sulci was generally delayed from 8 to 14 s. This larger delay is consistent with the longer time required for blood to reach the larger vessels. Finally, stimulus-induced NMR phase changes were observed for the largest vessels, which are attributed to bulk susceptibility shifts.

Key words: brain mapping; BOLD; spiral scanning; time-lag imaging.

INTRODUCTION

Stimulus-induced contrast changes in magnetic resonance images are providing a unique noninvasive tool for studying human brain function. The ability to map neural activity with high spatial resolution is of great interest both to clinicians and neuroscientists. Clinical applications include localization of epileptic foci, presurgical mapping of normal brain function, and elucidation of function in the diseased brain. For neuroscientists, the ability to do a noninvasive single-subject experiment has accelerated the study of different functional areas of the human brain and their interconnections.

Brain activation contrast results from the hemodynamic response to neural activity. Fox *et al.* showed that increases in both cerebral blood volume and flow overcompensate for modest increases in oxygen extraction, which results in a localized increase in blood oxygenation (1). The magnetic susceptibility of oxygenated hemoglobin is closer to that of the surrounding tissue and plasma than the displaced deoxygenated blood, which results in a local decrease in T_2^* dephasing. Consequently, regions of activated cortex display a signal magnitude increase in gradient-recalled echo images. This basic mechanism has been termed blood-oxygenation-level-dependent (BOLD) contrast (2). It was first observed *in vivo* by Ogawa *et al.* in the rodent brain at 7 T and 8.4 T. The first stimulus-induced BOLD contrast-change experiments in humans were performed by Kwong *et al.* using photic stimulation of the visual cortex (3).

Although many groups now obtain reproducible brain activation data, and a remarkable amount of progress has been made both in neuroscience and clinical applications, the vascular structures that are responsible for the observed signal changes have not been unambiguously identified. Lai *et al.* have reported that activation near the central sulcus resulting from motor stimulus at 1.5 T can be traced to the large pial vein that runs along the sulcus (4). Other groups report activation that is spatially correlated with both gray matter and macroscopic veins in sulci at 1.5 T and 4 T (5, 6). The distinction between activation stemming from large veins running along sulci and smaller vessels in gray matter is an important one because veins that run along sulci receive blood from a large volume of cortex and therefore localize neural metabolism poorly. Unfortunately, these larger draining veins tend to produce the largest activation signals in gradient-echo MRI, which therefore may lead to incorrect conclusions in experiments having poor contrast-to-noise ratio.

Several techniques have been proposed to discriminate between signals that originate from large veins and signals generated in the gray matter. For example, it has been suggested that spin-echoes should give signal changes for small vessels, due to water diffusion during the echo period, but not for large veins (5, 7, 8). Also, Menon *et al.* have shown that gradient-recalled echo signal changes are a linear function of echo time for gray matter but not for identifiable veins (6).

We present an alternative approach, with data demonstrating that the time course of activation signals in the visual cortex contain a large amount of information about the source of the hemodynamic response to neural activity. Our main finding is that signals resulting from large vessels have larger temporal delays, in general, than those from gray matter. We suggest that these time delays are the result of transit-time effects as the oxygenated blood traverses the vasculature. Images of these delay times elucidate the hemodynamic response to neural activity and may be a powerful tool for discriminating against signals that originate from large veins. Bandettini *et al.* have previously used cross-correlation of activation response with the stimulation sequence in time-course

MRM 33:745–754 (1995)

From the Department of Radiology (A.T.L., G.H.G.), and the Department of Electrical Engineering (C.H.M.), Stanford University, Stanford, California.

Address correspondence to: Adrian T. Lee, Ph.D., Department of Radiology, Lucas MRS Center, 1201 Welch Road, Stanford, CA 94305–5488.

Received April 15, 1994; revised January 24, 1995; accepted January 25, 1995.

This work was funded in part by The Lucas Foundation, General Electric Medical Systems, and NIH grant R01-CA58590.

0740-3194/95 $3.00

experiments to derive additional statistical confidence in the activation, and have investigated various frequency-dependent activation phenomena (9). To the best of our knowledge, however, temporal response has not been previously suggested as a discriminate for activation source.

In addition to delay time, we describe another parameter that may help to localize large veins. This parameter describes the strength of NMR phase changes in response to the stimulus. BOLD phase changes were first explored by Wen *et al.* (10). Regions that show correlation at the temporal frequency of the stimulus coincide anatomically with large vessels. Voxels that have a high fractional blood volume may show phase changes due to bulk susceptibility shifts with oxygenation.

METHODS

Data Acquisition

Volunteers were imaged using a 1.5 T whole body system (General Electric Medical Systems Signa, Rev. 5.2) with a 5-inch diameter local receive coil. The head of the subject was fixed in place using a "bite-bar" that was formed with the individual's dental impression. Each scan consisted of 20 interleaved spiral-readout acquisitions (11). Spiral readouts have several advantages for brain-activation mapping. First, spiral readouts are relatively insensitive to motion artifacts that result from cardiac pulsatility (12, 13). With spin-warp techniques, a cardiac pulsation that occurs during collection of data near the origin of *k*-space results in a ghost artifact. In the case of spiral readouts, the origin of *k*-space is acquired at the beginning of each acquisition and the effect of a cardiac pulsation is reduced by the averaging of low spatial frequencies that occurs. Also, gradient moments of all orders are equal to zero from excitation until time *TE* and are periodically zeroed during readout with spiral acquisitions, which also reduces sensitivity to motion. Spiral readout trajectories make efficient use of gradient strength, which is another of their advantages. This efficiency allows fairly rapid acquisition of high spatial resolution images.

Gradient-echo spiral images were acquired every 1.5 s with a 188 × 188 image matrix, a field-of-view of 20 cm, a *TR* of 75 ms, a *TE* of 40 ms, and a flip angle of 23 degrees. The in-plane resolution was 1.06 × 1.06 mm, and slice thicknesses of 3 or 5 mm were used. The scan was run continuously, and 128 to 256 images were acquired for each experiment. Scan planes were chosen either parallel or perpendicular to the calcarine fissure. The raw data was transferred to a workstation for image reconstruction, which consisted of data gridding to a 256 × 256 *k*-space matrix and subsequent Fourier transform (11, 14). The phase of the NMR signal was calculated from the complex Fourier transform data using the relation ϕ_{NMR} = arctan (imaginary component/real component). Because phase wraps did not occur in the regions under study, phase unwrapping was not performed. Standard phase unwrapping algorithms could be implemented, however.

Visual stimuli were projected onto a screen at the end of the patient table. The volunteer viewed the screen via an adjustable mirror mounted adjacent to the bite-bar frame. The stimulus was a counter-face flickered radial checkerboard. The checkerboard flickered (black sections becoming white and visa versa) at a frequency of 10 Hz. The visual angle subtended by the diameter of the entire checkerboard was 20 degrees. The checkerboard was divided by eight equally spaced concentric rings and eight equally spaced radial lines. Stimulus-on periods of 18 s alternated with stimulus-off periods of 18 s. A Macintosh computer was used to generate the stimulus pattern. The scan was started at the beginning of the second stimulus cycle, because the response to the first cycle was qualitatively different from the rest (overshoot did not occur). The scan was started with the Macintosh computer or was manually started depending on whether the hardware interface with the Signa console was available. Several baseline images were taken before each activation experiment. T_1-weighted, flow-compensated, spin-warp anatomy images with 256 × 256 in-plane resolution were acquired during each experiment. Although 10 volunteers were scanned, all the data that will be shown are from one volunteer for consistency. Data from the other volunteers were qualitatively similar to the data presented here and will be discussed.

Data Analysis

The linear correlation between each pixel's time-course and sine and cosine functions at the frequency of the stimulus was calculated. The linear correlation has the important property that it indicates the statistical strength of the correlation between the two functions that it operates on. As a result, less significance is given to a time course that simply has a large noise component at the frequency of the stimulus. This is the same property that makes the paired *t* statistic more robust than a simple subtraction. Linear correlation of a time course is more efficient, however, because the sections of data where the hemodynamics have not reached equilibrium are also used. The linear correlation coefficient, which is also known as Pearson's *r*, is given by

$$r = \frac{\sum_{1}^{N} x_i y_i}{\sqrt{\left(\sum_{1}^{N} x_i^2\right)\left(\sum_{1}^{N} y_i^2\right)}}, \quad (1)$$

where *r* ranges from −1 to 1, x_i is the signal magnitude, y_i is the value of the comparison function, and N is the number of images. Sinusoids were chosen as the comparison function because the temporal low-pass filtering that occurs due to the hemodynamic response time combined with the 36-s stimulus period results in a Fourier power spectrum with nearly all its power at the frequency of the stimulus. (For a single-pole low-pass filter with a 3-s time constant >90% of the Fourier power would be contained in the fundamental.) The frequency of the stimulus was chosen to be just below the "elbow"

of the hemodynamic frequency response. Using the time course of selected pixels as the comparison function gave higher correlations, but also introduced artifactual activations in vessels such as the transverse sinus. Bandettini *et al.* have noted this effect using motor stimulation (9). The time course of activated pixels may contain Fourier components resulting from respiratory motion and cardiac pulsatility that have been aliased. Using such time courses as comparison functions may result in high correlations for regions that are particularly susceptible to pulsatility artifacts such as CSF. Figures 1d and 1e show two time courses fit to sinusoids (fits are for illustrative purposes only and were done with a least square minimization). Before the calculation of the correlation, each time course was fitted to a straight line, and this "trend" line was subtracted from the data. A sine and cosine correlation for each pixel was calculated from the expressions

$$r_s = \frac{\sum_1^N x_i \sin(\omega t_i)}{\sqrt{\left(\sum_1^N x_i^2\right)\left(\sum_1^N \sin^2(\omega t_i)\right)}} \quad (2)$$

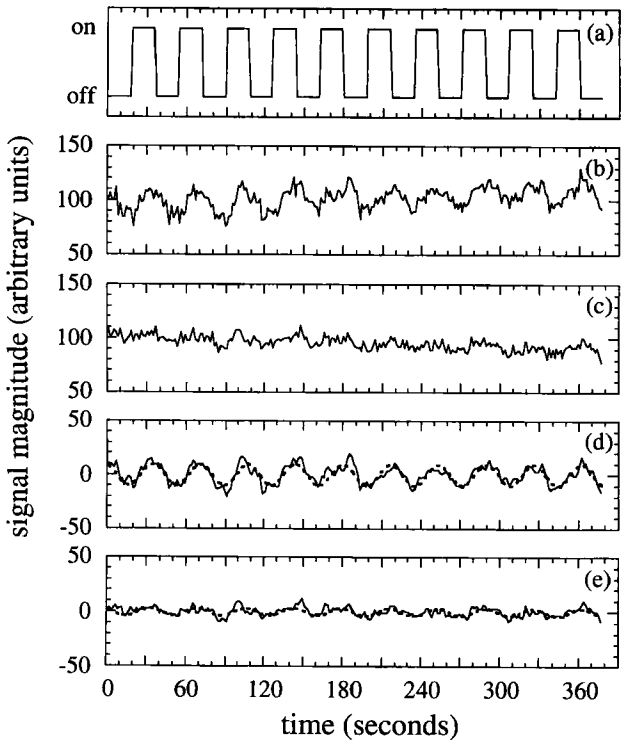

FIG. 1. (a) Time course of stimulus, which consisted of a circle filled with flashing squares in the "on" state and a blank field in the "off" state. NMR magnitude as a function of time for a region that is anatomically correlated with a large vessel (b) and with gray matter (c). The values from five adjacent pixels were averaged together and the data was low-pass filtered to improve the signal-to-noise ratio for display purposes. (d) and (e) Same data as in (c) and (d), but with trend lines subtracted and fitted to sinusoids (fits are for illustrative purposes only and were done with a least square minimization).

and

$$r_c = \frac{\sum_1^N x_i \cos(\omega t_i)}{\sqrt{\left(\sum_1^N x_i^2\right)\left(\sum_1^N \cos^2(\omega t_i)\right)}}, \quad (3)$$

where ω is the angular frequency of the stimulus, and t_i is the start time of each image. The magnitude and temporal phase of the correlation are given by

$$r_m = \sqrt{r_s^2 + r_c^2} \quad (4)$$

and

$$\phi_r = \tan^{-1}\left(\frac{r_s}{r_c}\right), \quad (5)$$

where r_m ranges from 0 to 1 and ϕ_r ranges from 0 to 2π. The magnitude and temporal phase of the correlation were saved as images. An image was formed with the Fourier power at the stimulation frequency. The peak-to-peak signal swings compared with baseline can be calculated directly from this image and a baseline image. Figure 2 shows an anatomy image, a correlation image, a percentage signal deviation image, and a temporal phase image from the same experiment.

RESULTS

Temporal Phase Analysis

A scatterplot of peak-to-peak signal amplitude as a function of temporal phase for one volunteer is shown in Fig. 3. The signal amplitude is expressed as a percentage of baseline magnitude. In the plot each point represents a pixel with $r_m > 0.2$. The origin corresponds to the phase of the stimulus in this plot. The phase represents the temporal lag of each pixel's response. Because the period of the stimulus was 36 s, 10 degrees of phase corresponds to 1 s of temporal lag. There are two groups of data that are separated by roughly 180 degrees. The first group represents pixels that have a signal increase with stimulus and the second represents those having a signal decrease with stimulus. The phase of well-correlated responses are spread over >60 degrees in the first group of data. Because EEG data indicate that neural activity in the visual cortex starts in less than half a second after stimulation, the large spread of temporal lags is most likely hemodynamic in origin (15). Oxygenated blood is delayed by the transit time through the cerebral vasculature to a degree that depends on how far it has traveled from the site of flow regulation. In general, larger veins are further from the regulation site and should therefore give larger temporal delays. Variations in metabolic response time can also affect the temporal delay, but Silver has found that increases in blood flow occur within a narrow time window (1–2 s after stimulation) (16). The difference in phase between the stimulus and the signal has two components. The first is the delay of the response, and the second depends on the time-to-peak of

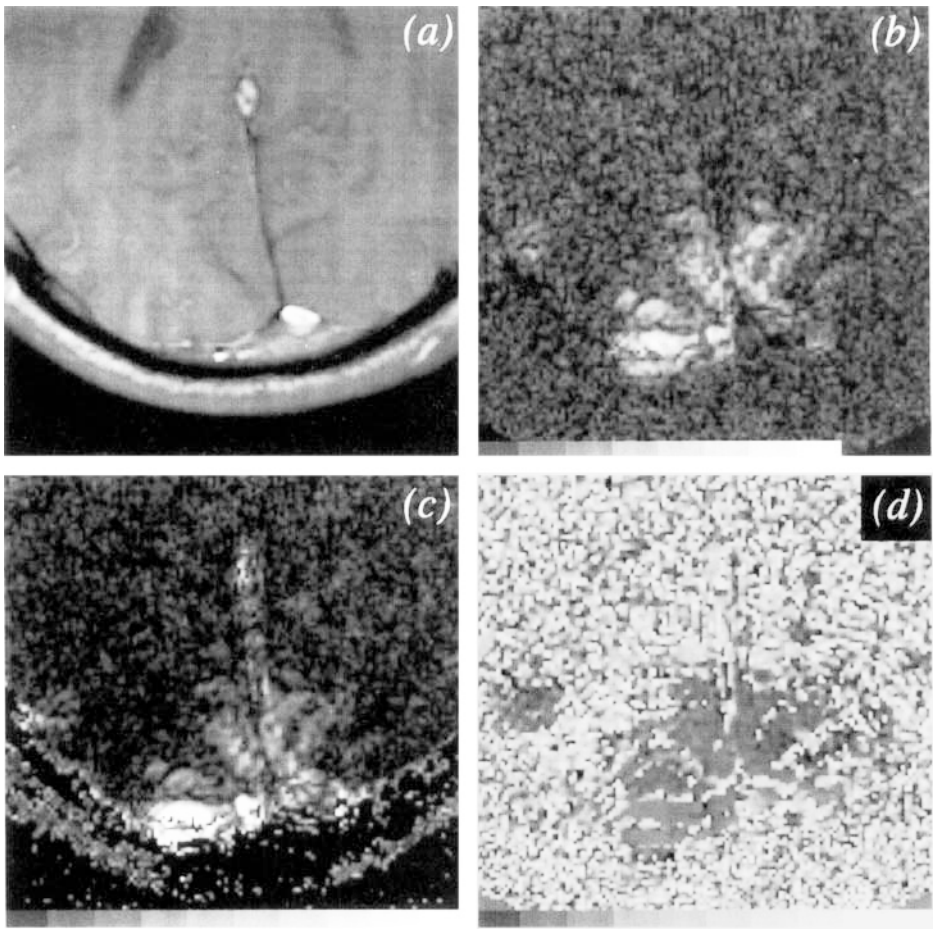

FIG. 2. (a) T_1-weighted, flow-compensated, spin-warp anatomy image. Original FOV = 20 cm and original image matrix = 256 × 256. Shown cropped to 10 cm × 10 cm with interpolation to 256 × 256. Slice thickness = 5 mm, *TR* = 500 ms, and *TE* = 31 ms. (b) Magnitude of correlation between sinusoid and time-course of each pixel. Scale shown at bottom contains values from 0.1 to 0.8. Maximum correlation = 0.77. Data set contains 252 images. (c) Peak-to-peak signal swing as a percentage of baseline image value. Scale shown contains values from 2% to ≥20%. (d) Phase of correlation between sinusoid and time-course of each pixel. Scale shown contains values from 36 to 360 degrees. Phase of stimulus is equal to 0 degrees.

the response. The second term can be described as the phase response of a low-pass frequency domain filter. If the rise-time and fall-time of the response are similar then the phase difference is given roughly by the delay plus one half the time-to-peak. In general, both the delay and the time-to-peak are affected by the continuum of transit times resulting from multiple discrete sources of oxygenated blood.

One important feature of Fig. 3. is that the maximum signal deviation tends to become monotonically larger with increasing phase for phase <100 degrees. For vessels with radius >8 μm, Ogawa *et al.* have calculated that the signal deviation should be proportional to the fractional blood volume in the voxel (17). Because the fractional blood volume of a voxel generally increases with the size of the contained vessels, an increase in maximum signal deviation with phase is consistent with an increase of temporal delay with vessel size. The range of signal deviations at each phase is probably due to a number of effects including: partial voluming of tissue, varying levels of neural metabolism, and veins that drain partially activated regions. It should be noted that the short repetition period of the pulse sequence used leads

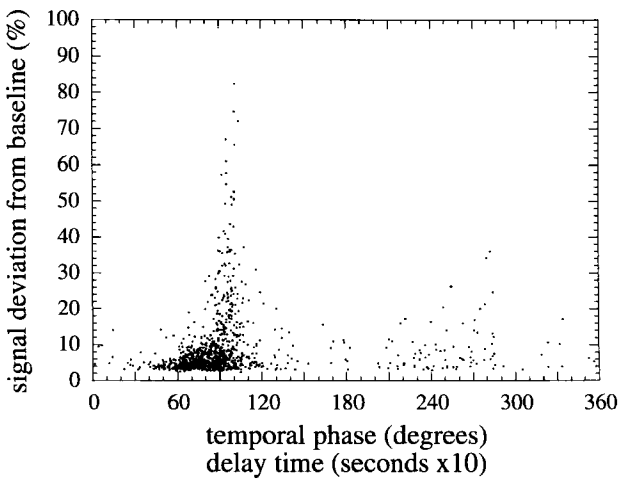

FIG. 3. (a) Peak-to-peak signal deviations given as a percentage change from baseline versus temporal phase. Very large deviations with temporal phase >80 degrees correspond to a region that is anatomically correlated with a large vessel. This region had a very low baseline magnitude. Only pixels with correlation >0.2 are shown.

to in-flow effects that augment the signal deviations as was first shown by Duyn *et al.* (18). This in-flow effect leads to large signal deviations in the case of large veins. All the high percentage signal changes with 90 < phase < 110 degrees are almost certainly due to large veins. (The very large percentage changes come from a region beyond the posterior edge of the right hemisphere where the baseline magnitude was very low.) Simply disregarding pixels with large signal deviations will not eliminate all signals resulting from large veins, however, due to the range of signal deviation at each phase. Scatterplots of signal deviation versus phase for all the volunteers showed similar features to the one shown in Fig. 3, although they varied in the ratio of short (phase < 80 degrees) to long (80 < phase < 110 degrees) delay activation. For some experiments, there was an absence of short-delay voxels, which might indicate that all the activation was due to large veins in those cases (the activated cortex is presumably in adjacent slices).

Subsets of the correlation image shown in Fig. 2b can be constructed using the phase image as a control to show the location of pixels with a particular range of phase. In Fig. 4, four correlation images that include pixels with progressively higher phase are shown. It can be seen from comparison with the underlying anatomy image that pixels with phase >80 degrees (Figs. 4c and 4d) appear to correspond largely to visible vessels and sulci (sulci contain pial vessels). Pixels with phase <80 degrees appear to correspond largely to regions of gray matter (see Figs. 4a and 4b). The activated regions with phase >80 degrees are wider than the expected width of vessels. Widening of activated regions by vessels might result from a "blooming" effect due to extravascular gradients. It should be noted that natural variability of vascular structure such as the presence of shunts might lead to variations in temporal phase. If these are large enough, the identification of vascular structures would become inaccurate. Also, arterial vessels may give activation signals due to the in-flow effect. This might account for some of the early onset data that are anatomically correlated with visible vessels. The use of presaturation bands might eliminate this problem.

Large veins may carry oxygenated blood that originated several centimeters away from the pixel location, including regions in adjacent slices. In fact, very large vessels that are visible on slices perpendicular to the calcarine fissure have phase differences of up to 140 degrees in the first group. In Fig. 4e pixels with 200 < phase < 260 degrees are shown. These signals are roughly 180 degrees out of phase with the first group of data, indicating a signal decrease with stimulation. Most of these out-of-phase voxels are anatomically correlated with large vessels. Data from other volunteers are similar; usually there is a second group of data that is 180 degrees out of phase from the primary group. In subsequent experiments, we have also varied the stimulus period. Stimulus-on periods of 10, 20, and 40 s were tried (off-period equal to on-period), with all experiments yielding a 180-degree out-of-phase signal group. This indicates that these signals are not simply time delayed by 180 degrees. The origin of these signal changes is not clear, but it is possible that the signal decreases could be caused by flow effects or that the vessel is draining tissue that has an oxygenation decrease with stimulation. Also, increased metabolic activity in one area may result in a redirection of the flow of oxygenated blood resulting in oxygenation decreases in other areas.

Flow Visualization

The flow of oxygenated blood in the vasculature is apparent when viewing a movie of correlation images that have been filtered with respect to temporal phase. A time sequence was made using a 10-degree (1 s) wide phase window where each successive image had phase boundaries that were incremented by 2 degrees (200 ms). This movie showed movement of activation that could be due to flow along large veins. In one activation path adjacent to the sagittal sinus, the velocity of the phase change corresponded to a flow velocity of ~1 cm/s (see Fig. 4).

Uncertainty in Temporal Phase

The uncertainty in the temporal phase has a systematic and a statistical term. The statistical term, which results from noise in the magnitude data, can be approximated using the fact that a z-score with a known standard deviation can be formed with the correlation. The z-score and its standard deviation are given by ref. 19

$$z = \frac{1}{2}\ln\left(\frac{1 + r_m}{1 - r_m}\right) \tag{6}$$

and

$$\sigma_z \sim \frac{1}{\sqrt{N-3}}. \tag{7}$$

From these two quantities the uncertainty in the phase can be calculated and is given by

$$\sigma_\phi \sim \frac{(1 - r_m^2)}{r_m^2}\frac{1}{\sqrt{N-3}}, \tag{8}$$

where σ_ϕ is given in radians and decreases quadratically with r_m. By measuring the phase for each cycle of the stimulus, the standard deviation of the phase in the data can be measured. The experimental standard deviations agree well with the calculated values indicating that the phase error is dominated by statistics. For example, at $r_m = 0.4$ ($N = 252$) both the calculated standard deviation in phase and the average measured standard deviation in phase are ~0.33 radians, which corresponds to an uncertainly in time of ~1.9 s. To form an image that includes all the activation due to gray matter, a phase cutoff that depends on the correlation must be used. In Fig. 5 pixels with phase equal to 60 degrees $\pm 2\ \sigma_\phi$ are shown in red. All other activated pixels are shown in blue. ($r_m > 0.175$ for both red and blue pixels.) The central phase value of 60 degrees was chosen to eliminate voxels that are anatomically correlated with large vessels. The red regions include early onset activation to 90% confidence, but also contain some late onset activation. The blue regions include only late onset activation to 90% confidence. This analysis is useful for evaluating the extent of an

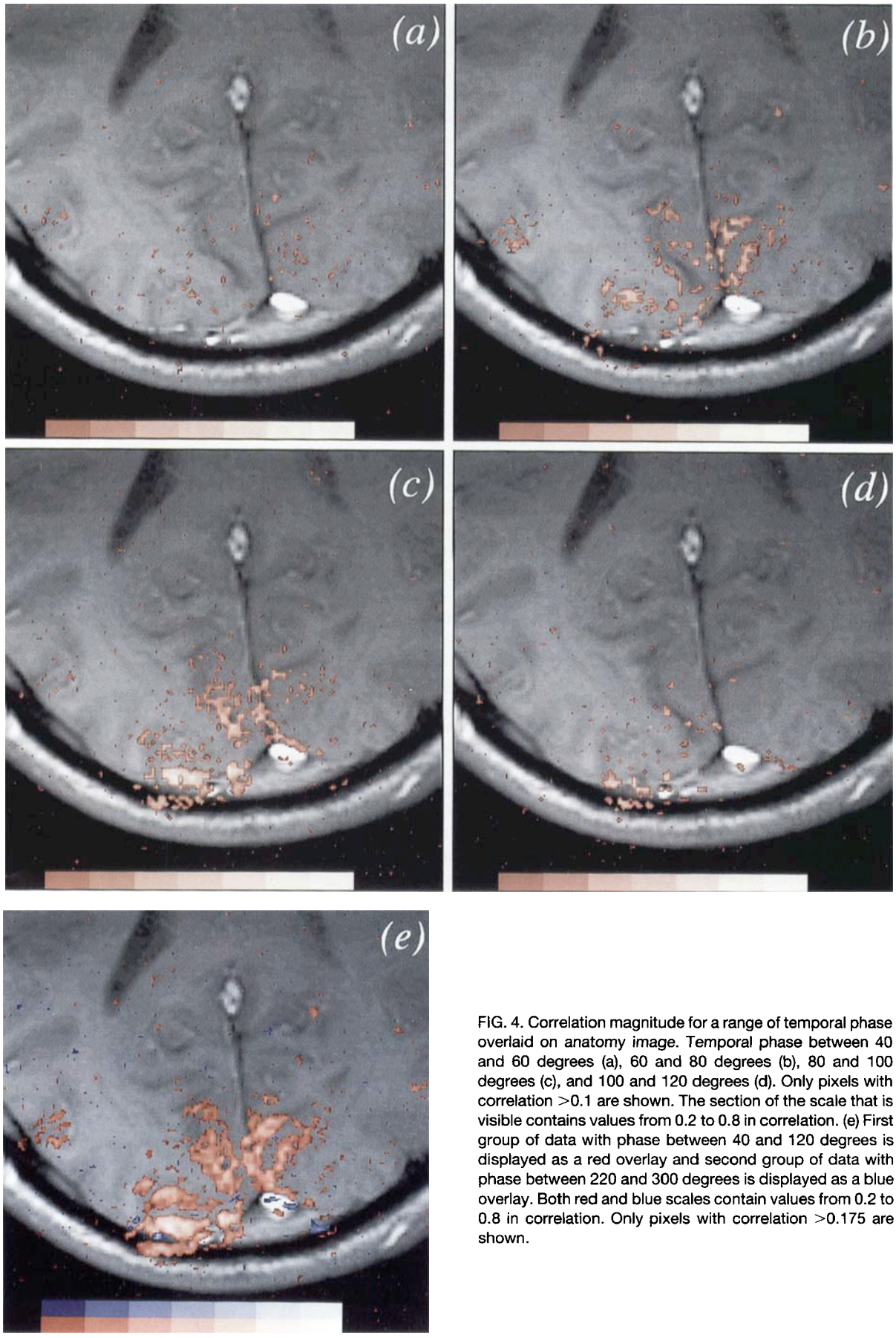

FIG. 4. Correlation magnitude for a range of temporal phase overlaid on anatomy image. Temporal phase between 40 and 60 degrees (a), 60 and 80 degrees (b), 80 and 100 degrees (c), and 100 and 120 degrees (d). Only pixels with correlation >0.1 are shown. The section of the scale that is visible contains values from 0.2 to 0.8 in correlation. (e) First group of data with phase between 40 and 120 degrees is displayed as a red overlay and second group of data with phase between 220 and 300 degrees is displayed as a blue overlay. Both red and blue scales contain values from 0.2 to 0.8 in correlation. Only pixels with correlation >0.175 are shown.

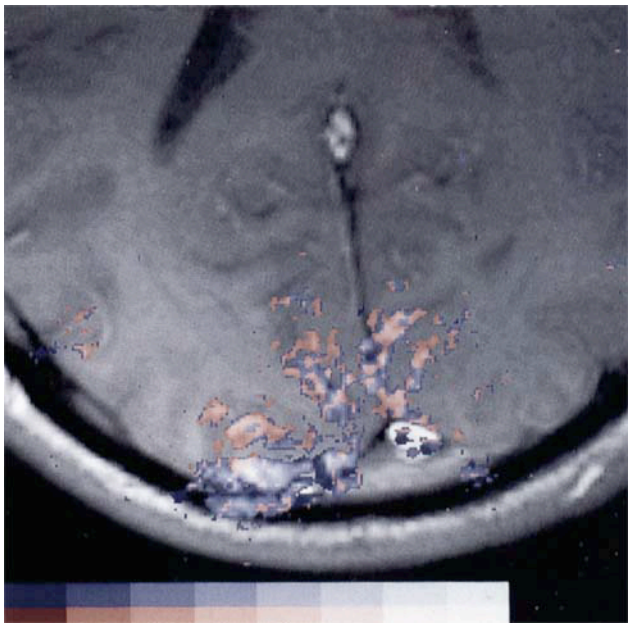

FIG. 5. Correlation magnitude classified by temporal phase. Red pixels represent the correlation of points that have a temporal phase of 60 degrees ± $2\sigma_\phi$ (see text for details). Blue pixels represent all the pixels with correlation >0.175 that are not red pixels. Blue pixels are late in onset to 90% confidence level. The sections of the color scales that are visible contain values from 0.2 to 0.8 in correlation.

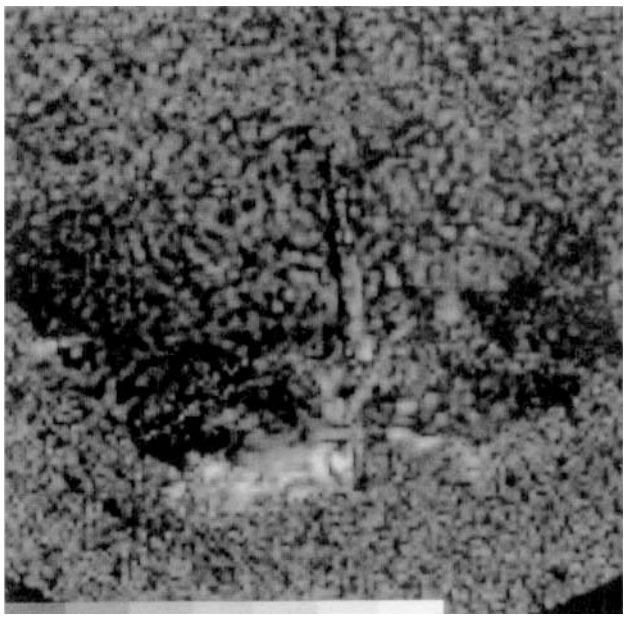

FIG. 6. Magnitude of correlation between sinusoid and time-course of each pixel's NMR phase. Scale shown at bottom contains values from 0.1 to 0.7. Maximum correlation = 0.63. Data set contains 252 images.

activated area, since much of the early onset activation has a relatively low correlation.

NMR Phase Image

In addition to the NMR magnitude, the NMR phase also shows deviations in response to stimulation as was first demonstrated by Wen *et al.* (10). Susceptibility-induced phase changes were also observed in early bolus injection work (20). The time course of each pixel's NMR phase was correlated with sine and cosine functions at the stimulation frequency in the same manner as was done for the magnitude. Figure 6. shows an image of the correlation coefficient, r_ϕ. Regions with a high value of r_ϕ appear to be anatomically correlated with large vessels. Figure 7. shows a plot of peak-to-peak NMR phase change as a function of temporal phase. Almost all the activation in the in-phase group occurs with greater than 80 degrees of temporal phase, which coincides with the late onset activation in the magnitude data. The out-of-phase group is roughly 180 degrees out of phase with the in-phase group. In Fig. 8, activated regions from the first group are shown in red and regions from the second group are shown in blue. Phase changes probably occur predominantly in pixels that have a high blood volume fraction, where the susceptibility of a large fraction of the voxel can change. The difference in susceptibility between oxygenated and deoxygenated blood $\Delta\chi$ was measured by Ogawa and Lee as 0.1 ppm (21). The phase change due to changes in oxygenation can be approximated by

$$\Delta\phi_{\mathrm{NMR}} \sim F\,\Delta\chi\,\omega_0\,\Delta Y\,f_b\,TE, \tag{9}$$

where ω_0 is the proton resonance frequency at 1.5 T, ΔY is the fractional change in oxygenation, f_b is the fraction of the pixel volume that contains blood, TE is the echo time, and F is a form factor that depends on the shape and the orientation of the vessel. The maximum phase change of ~3 degrees in the data, corresponds to $\Delta Y \sim 0.033$ for $f_b = 1$. The origin of the second group of data is unclear, but the negative phase shifts might result from increased flow rates in the presence of small residual gradients during the echo period.

Pixels with a strong NMR phase response, but with a weak magnitude response probably contain a large vein. Similarly, pixels with a strong NMR magnitude response, but with a weak phase response probably contain many small vessels. Discrimination of large veins might be accomplished by examining the ratio of the phase response to the magnitude response. We define

$$\theta_{\phi m} = \tan^{-1}\left(\frac{r_\phi}{r_m}\right) \tag{10}$$

where $\theta_{\phi m}$ ranges from 0 degrees, for pure magnitude response, to 90 degrees, for pure phase response. In Fig. 9 a map of $\theta_{\phi m}$ is shown overlaid on the anatomy image. Regions with a high value of $\theta_{\phi m}$ appear to correlate anatomically with large vessels. In Fig. 10, pixels with $\theta_{\phi m} < 12$ degrees are shown in red, and pixels with $\theta_{\phi m} \geq 12$ degrees are shown in blue. This image shows a great deal of similarity to the image based on the temporal phase of the magnitude (Fig. 5), but is different in several regions. For example, there is a small region near the back of the right hemisphere that is blue in Fig. 5, but red in Fig. 10. The temporal phase method is probably more accurate here, because this region correlates anatomically with a large vessel.

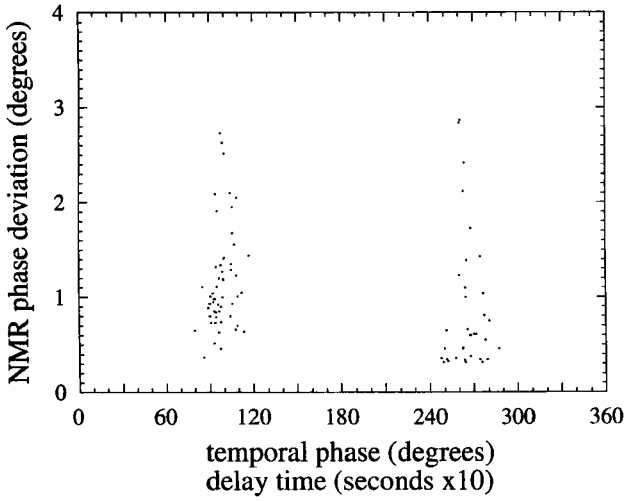

FIG. 7. Peak-to-peak NMR phase deviation as a function of temporal phase of NMR phase. The range of temporal phase corresponds closely to that of the late onset NMR magnitude data. Only pixels with magnitude of correlation between the NMR phase time-course and sine and cosine functions >0.35 are shown. Some pixels with lower correlation had phase deviations of up to 8 degrees, but their response was temporally uncorrelated with the stimulus.

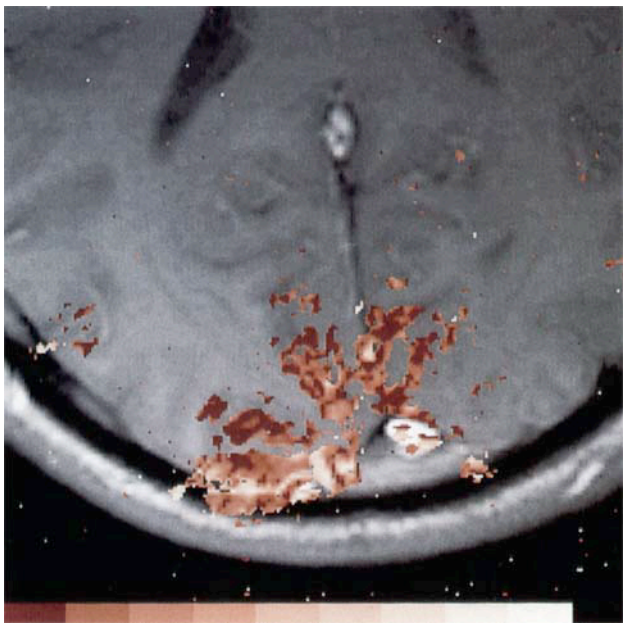

FIG. 9. Angle $\theta_{\phi m}$ between NMR phase correlation coefficient, r_ϕ, and NMR magnitude correlation coefficient, r_m. Pixels shown overlaid on anatomy image have $r_\phi > 0.2$ and/or $r_m > 0.2$. Scale shown contains $\theta_{\phi m}$ values from 10 to 90 degrees.

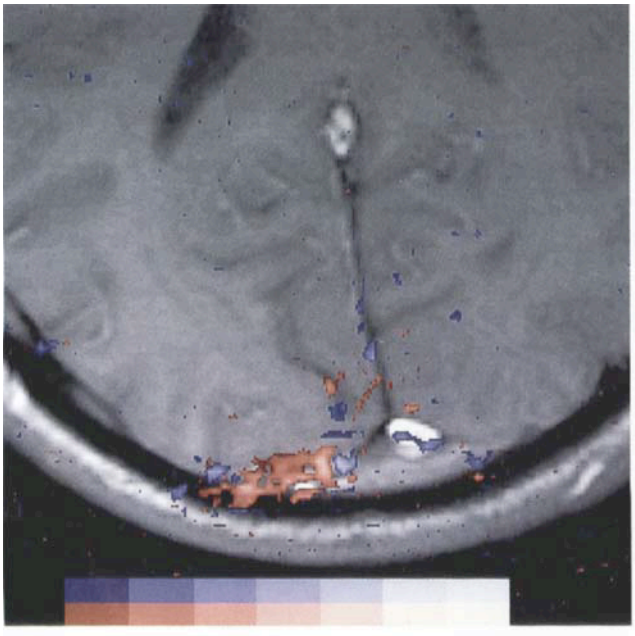

FIG. 8. Magnitude of correlation between the time-course of the NMR phase and sine and cosine functions. Red and blue pixels represent the in-phase and out-of-phase groups respectively. Only pixels with correlation >0.2 are shown overlaid on anatomy image, and the scale contains values from 0.2 to 0.8. Maximum correlation is 0.63.

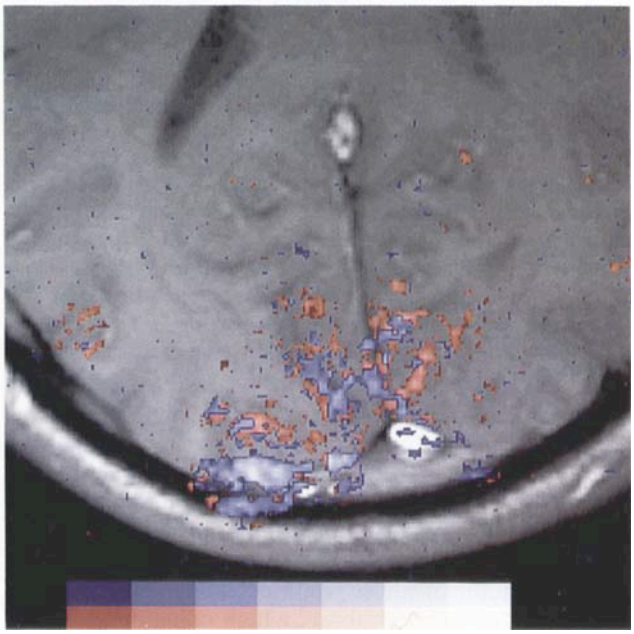

FIG. 10. NMR magnitude correlation classified by $\theta_{\phi m}$, the angle between r_ϕ and r_m. Only pixels with $r_\phi > 0.2$ and/or $r_m > 0.2$ are shown overlaid on anatomy image. Pixels with $\theta_{\phi m} < 12$ degrees are shown in red and those with $\theta_{\phi m} \geq 12$ degrees are shown in blue. Scale shown contains r_m values from 0.1 to 0.8.

DISCUSSION

It has become clear that BOLD contrast changes are the result of oxygenation changes in a range of vessel sizes. The localization of metabolic activity becomes less accurate with increasing vein radius, because the volume of cortex that the vein serves increases. Pial veins run along the surface of cortex and have diameters of 100 to 400 μm (22). In general, they serve relatively large volumes of cortex and therefore localize activity poorly. Pial veins are not always apparent on standard-resolution anatomy images, which means that activation signals from them can often be misinterpreted. Cortical tissue contains a range of vessel sizes from capillaries to 100 μm diameter

intracortical veins. The intracortical veins resemble inverted trees where the "trunks" connect to pial veins at the surface of the cortex. The volume that each vein drains depends on the size of the vein. Duvernoy *et al.* find that the largest intracortical veins serve conically shaped "units" that are 1 to 4 mm in diameter at their widest and about 3 mm in depth (22). Intermediate size intracortical veins serve units of 0.75 to 1 mm in diameter with depths of 1 to 2 mm. Roughly 75% of the blood in the brain is contained in venous vessels, whereas only 5% of the blood is contained in capillaries. It is likely, therefore, that a significant part of the stimulus-induced signal change results from oxygenation changes in intracortical and pial veins.

We have compared MR angiograms (MRAs) with activation maps. In general, the vessels visible in MRAs are also conspicuous in the T_1-weighted anatomy images, and we have found no particular advantage to the use of MRA (even using magnetization transfer background suppression) over T_1 images. Unfortunately, most of the vessels that are involved in cortical BOLD contrast are too small to detect with these conventional MR imaging techniques. Vessels that *can* be observed in the T_1 images correlate well with the hemodynamic model in that their activation response is significantly delayed (see Fig. 4).

Two techniques have been presented that discriminate activation associated with pial and larger veins. In the first, we have found that activation in the visual cortex lags the stimulation by a wide range of delay times (4 to 14 s). The signals that are the most delayed correspond anatomically to macroscopic blood vessels and typically have a strong correlation magnitude. Movies of the temporal activation sequence of NMR magnitude show blood flow with velocities consistent with vessels. Interestingly, subtle flow effects are evident in these time sequences that would not be detectable with conventional MR flow measurements.

All of these effects are consistent with the hemodynamic transit-time model for blood flow. The earliest signals are therefore presumed to result predominantly from activation within the cortical parenchyma itself. In the second technique, we examined the NMR phase response and found that regions with a significant amount of response corresponded anatomically with blood vessels. Pixels with a significant blood volume fraction can have NMR phase shifts due to changes in bulk susceptibility.

The fact that many of the same areas are identified with both methods, despite the fact that the methods rely on independent mechanisms, gives confidence that the underlying assumptions are reasonable. The temporal phase method has the advantage of being less sensitive to partial volume effects than the other two methods. If activated tissue and nonactivated tissue are contained in the same voxel, the magnitude and phase response will be different from that of a voxel containing only activated tissue. Although the magnitude response is weaker in the mixed voxel, the temporal phase of the magnitude response should be unaltered. It is possible that combining the two methods might lead to more accurate discrimination than with a single method. Also, both methods would probably become more accurate at higher magnetic fields. Compared with existing methods, the two presented here have the advantage of requiring only one echo per repetition period.

The interleaved spiral pulse sequence simultaneously gives high temporal and spatial resolution in addition to low sensitivity to cardiac pulsatility. It also has the advantage of not requiring specialized gradient hardware and wideband receivers. An additional advantage is that the result of motion with spiral sequences is blurring rather than ghosting. Moreover, correlation of the time-course data with a periodic comparison function gives further rejection of motion artifacts and results in a high statistical significance for activated regions. Finally, it should be noted that many of the voxels that are identified as containing a large vessel may also contain activated cortical tissue. Without higher spatial resolution images, however, it would probably be very difficult to determine which of the pixels that contain a large vein also contain activated cortical tissue.

ACKNOWLEDGMENTS

The authors thank their collaborators in the Departments of Psychology and Neurology: E. J. Chichilnisky, S. E. Engel, W. T. Newsome, D. E. Rumelhart, M. N. Shadlen, and B. A. Wandell for their participation; and T. J. Brosnan, J. O. Fredrickson, G. B. Pike, and G. A. Wright for their help.

REFERENCES

1. P. T. Fox, M. E. Raichle, M. A. Mintun, C. Dence, Nonoxidative glucose consumption during focal physiologic neural activity. *Science* **241,** 462 (1988).
2. S. Ogawa, T. M. Lee, A. S. Nayak, P. Glynn, Oxygenation-sensitive contrast in magnetic resonance image of rodent brain at high magnetic fields. *Magn. Reson. Med.* **14,** 68 (1990).
3. K. K. Kwong, J. W. Belliveau, D. A. Chesler, I. E. Goldberg, R. M. Weisskoff, B. P. Poncelet, D. N. Kennedy, B. E. Hoppel, M. S. Cohen, R. Turner, Dynamic magnetic resonance imaging of human brain activity during primary sensory stimulation. *Proc. Natl. Acad. Sci. (USA)* **89,** 5675 (1992).
4. S. Lai, A. L. Hopkins, E. M. Haacke, D. Li, B. A. Wasserman, P. Buckley, L. Friedman, H. Meltzer, P. Hedera, R. Friedland, Identification of vascular structures as a major source of signal contrast in high resolution 2D and 3D functional activation imaging of the motor cortex at 1.5T: preliminary results. *Magn. Reson. Med.* **30,** 387 (1993).
5. P. A. Bandettini, E. C. Wong, A. Jesmanowicz, R. S. Hinks, J. S. Hyde, Simultaneous mapping of activation-induced $\Delta R2^*$ and $\Delta R2$ in the human brain using a combined gradient-echo and spin-echo EPI pulse sequence, *in* "Proc. SMRM, 12th Annual Meeting, New York, 1993," p. 169.
6. R. S. Menon, S. Ogawa, D. W. Tank, K. Ugurbil, Tesla gradient recalled echo characteristics of photic stimulation-induced signal changes in the human primary visual cortex. *Magn. Reson. Med.* **30,** 380 (1993).
7. R. Turner, P. Jizzard, D. L. Bihan, A. Prinster, Contrast mechanisms and vessel size effects in BOLD contrast functional neuroimaging, *in* "Proc., SMRM, 12th Annual Meeting, New York, 1993," p. 173.
8. K. K. Kwong, D. A. Chesler, C. S. Zuo, J. L. Boxerman, J. R. Baker, Y. C. Chen, C. E. Stern, R. M. Weisskoff, B. R. Rosen, Spin-echo (T2,T1) studies for functional MRI, *in* "Proc., SMRM, 12th Annual Meeting, New York, 1993," p. 172.

9. P. A. Bandettini, A. Jesmanowicz, E. C. Wong, J. S. Hyde, Processing strategies for time-course data sets in functional MRI of the human brain. *Magn. Reson. Med.* **30,** 161 (1993).
10. H. Wen, S. Wolff, K. Berman, R. Turner, M. Iadarolla, R. Balaban, Phase and magnitude functional imaging of motor tasks and pain stimuli, *in* "Proc., SMRM, 12th Annual Meeting, New York, 1993," p. 9.
11. C. H. Meyer, B. S. Hu, D. G. Nishimura, A. Macovski, Fast spiral coronary artery imaging. *Magn. Reson. Med.* **28,** 202 (1992).
12. D. C. Noll, C. H. Meyer, J. D. Cohen, W. Schneider, Spiral scan imaging of cortical activation, *in* "Proc., SMR, 12th Annual Meeting, San Francisco, 1993," p. 44.
13. G. H. Glover, A. T. Lee, C. H. Meyer, Motion artifacts in fMRI: comparisons of 2DFT with PR and spiral scan methods, *in* "Proc., SMRM, 12th Annual Meeting, New York, 1993," p. 197.
14. J. I. Jackson, C. H. Meyer, D. G. Nishimura, A. Macovski, Selection of a convolution function for Fourier inversion using gridding. *IEEE Trans. Med. Imaging* **10,** 473 (1991).
15. B. Rockstroh, T. Elbert, A. Canavan, W. Lutzenberger, N. Birbaumer, "Slow Cortical Potentials and Behavior," Urban and Schwarzenberg, Baltimore, 1989.
16. I. A. Silver, Cellular microenvironment in relation to local blood flow, "Cerebral Vascular Smooth Muscle and its Control," Elsevier/Excerpta Medica, Amsterdam, 1978.
17. S. Ogawa, R. S. Menon, D. W. Tank, S. G. Kim, H. Merkle, J. M. Ellermann, K. Ugurbil, Functional brain mapping by blood oxygenation level-dependent contrast magnetic resonance imaging. A comparison of signal characteristics with a biophysical model. *Biophys. J.* **64,** 803 (1993).
18. J. H. Duyn, C. T. W. Moonen, R. W. d. Boer, G. H. v. Yperen, P. R. Luyten, Inflow versus deoxyhemoglobin effects in "BOLD" functional MRI using gradient echoes at 1.5 T, *in* "Proc., SMRM, 12th Annual Meeting, New York, 1993," p. 168.
19. W. H. Press, B. P. Flannery, S. A. Teukolsky, W. T. Vetterling, "Numerical Recipes in C," Cambridge University Press, Cambridge, U. K., 1988.
20. T. E. Conturo, P. B. Barker, V. P. Matthews, L. H. Monsein, R. N. Bryan, MR imaging of cerebral perfusion by phase-angle reconstruction of bolus paramagnetic-induced frequency shifts. *Magn. Reson. Med.* **27,** 375 (1992).
21. S. Ogawa, T. M. Lee, Magnetic resonance imaging of blood vessels at high fields: in vivo and in vitro measurements and image simulation. *Magn. Reson. Med.* **16,** 9 (1990).
22. H. M. Duvernoy, S. Delon, J. L. Vannson, Cortical blood vessels of the human brain. *Brain. Res. Bull.* **7,** 519 (1981).